

MODEL FORM UNCERTAINTY REPRESENTATION TO ENABLE MULTIFIDELITY DESIGN OF ADVANCED CONCEPTS

Henry D. Schwartz, Dimitri N. Mavris

Aerospace Systems Design Laboratory, Georgia Institute of Technology, Atlanta, GA 30332 USA

Keywords: *uncertainty characterization, Gaussian process, ensemble methods, likelihood ratio*

Abstract

There has been a recent push by industry and government to make commercial air travel more environmentally friendly by striving to meet aggressive fuel burn, noise, and emissions goals simultaneously. This has forced engineers to move away from traditional turbofan engines mounted on tube-and-wing aircraft, and look toward advanced concepts. The development of advanced concepts requires engineers to utilize parametric design space exploration techniques to facilitate their understanding of the concept. The research presented in this paper focuses on formulating a stochastic method to enable parametric design space exploration for advanced concepts by creating an accurate representation of the high fidelity design space. As an initial step, the method is implemented on NACA 4-series airfoils as a proof of concept. The results indicate that using an ensemble method to combine Gaussian process surrogates of multiple data sets gives an improved high fidelity design space representation. Finally, rapid visualizations of the dynamic sensitivity derivatives enables the parametric exploration of the high fidelity design space.

Nomenclature

\underline{x}	vector of sample point locations
\underline{y}	vector of observed responses
f	model response
\hat{y}	kriging predictor
μ	mean
σ^2	variance

λ	hyperparameter
D	number of design parameters
n	number of observations
p, q	indices for the observations
l	design variable index
σ_n^2	noise variance hyperparameter
σ_f^2	signal variance hyperparameter
δ_{pq}	Kronecker delta
j	number of data sets
i	data set index
ε	Gaussian noise
\mathbf{f}^*	Gaussian process prediction distribution
β	variable weighting factor

1 Introduction

The rising cost of fuel along with increasing fears of climate change has caused governments and manufacturers to research more sustainable aircraft concepts. NASA has put forth aggressive goals to simultaneously decrease the fuel burn, noise, and emissions of commercial aircraft[1]. Many existing technologies have the ability to target one of these specific areas, but what makes this research area challenging is that these goals must be met simultaneously. Therefore, engineers must move away from traditional concepts. The development of advanced concepts can benefit greatly from the utilization of parametric design space exploration techniques which will enable engineers to gain a better understanding of a concept's behavior. Engineers must develop a strong understanding of the fundamental physics

behind a new concept during the conceptual design phase. The research presented in this paper focuses on formulating a method to enable parametric design space exploration for advanced concepts by creating an accurate representation of a high fidelity design space.

One advanced concept currently being researched by NASA and industry is the open rotor engine. Preliminary tests predict that the open rotor could reduce fuel burn by 20% to 30% compared to traditional turbofan engines[2]. The major difference between an open rotor engine and a traditional turbofan is the propulsor. The open rotor features two unducted counter-rotating blade sets. Removing the nacelle allows for higher bypass ratios without the additional drag penalty of large nacelles. Incorporating two blade rows allows engineers to achieve a given amount of thrust with a smaller diameter propeller which helps avoid losses due to high tip speeds. The counter-rotation of the blade rows mitigates the losses due to the tangential component of motion of the air behind the propeller. The individual blades are highly swept and constructed from advanced composite materials to allow for efficient operation at transonic speeds.

Despite the promising fuel burn benefit of the open rotor architecture, engineers are concerned about its ability to achieve the noise goal due to the lack of a nacelle. In order to meet the goals simultaneously, engineers need the capability to parametrically explore the design space. Parametric design space exploration techniques will enable them to perform trade studies to gain a better understanding of how changing a specific design parameter to reach a goal impacts the concept's ability to meet another goal. For example, an acoustics engineer may want to clip the aft blade row by 5% so the aft blades do not slice through the tip vortices of the front blades. This has a significant noise benefit, but it also adversely impacts the propulsive performance. Propulsion engineers need the ability to quickly create performance maps for use by an engine cycle analysis team to assess the system level performance of the quieter blade design. An accurate representation of a high fidelity design space will allow engineers to parametrically explore the

design space and quickly perform trade studies. For propulsion engineers conducting research on open rotor engines, this translates to a rapid parametric performance map generation tool.

Representing a high fidelity design space is challenging with advanced concepts such as the open rotor engine. Low fidelity potential flow computer simulations are not accurate in the transonic speed regime, and empirical models do not apply to this new generation of highly swept thin composite blades. Currently these maps are generated by fitting surrogate models to sparse high fidelity data sets along with the help of subject matter experts. This type of representation does not allow for the exploration of large areas of the design space. Improvements to the representation can be made by generating additional high fidelity data, but this requires more time and money which is typically not available.

One way of decreasing the computational effort and time associated with high fidelity simulations is to utilize information from multiple sources of data. These are commonly referred to as multifidelity methods in the literature[3, 4]. Multifidelity methods use a limited number of high fidelity simulations to augment the results from the low fidelity simulations. Surrogate models, or meta-models, can be used together with multifidelity methods to further decrease the computational and monetary burden of high fidelity testing[5, 6].

A decision maker must also have an understanding of the accuracy of the representation. A poor understanding of the uncertainty during the conceptual design phase leads to an increase in performance risk at the component level which leads to consequences at the system level. Thus, the high fidelity design space representation must also include uncertainty. Therefore, a probabilistic surrogate modeling technique should be used[7, 8]. Intuitively, the uncertainty of the surrogate model should grow as you move away from a known location. Oberkampf and Roy state that the uncertainty of experimental data should be represented with a Gaussian distribution, and the uncertainty should grow as a function of the distance from known observations[9]. Kennedy and O'Hagan believe data from computer exper-

iments should be treated in a similar manner[10]. Based on these observations, a Gaussian process regression is used to generate the surrogate models for this research. It should be made clear that the present research does not attempt to advance the state of the art of Gaussian processes. Rather it focuses on applying the mathematical concepts related to Gaussian processes to an applied engineering problem. A formal explanation of Gaussian processes is given in Section 2.2. Another reason for selecting a Gaussian process to generate the surrogate model is that the combination of Gaussian distributions results in another Gaussian distribution. Recall from earlier in this section that a key aspect of the proposed method involves the combination of multiple sources of data. Using Gaussian processes enables the use of ensemble methods to easily combine data sets. The resulting surrogate model is generated by fitting Gaussian processes to each data set individually and then combining them using an ensemble method. A formal explanation of the ensemble method used in this research is given in Section 2.3.

The resulting surrogate model corresponds to a high fidelity design space representation with the addition of uncertainty which enables the use of parametric design space exploration techniques. By dynamically visualizing the sensitivity derivatives, the decision maker is able to isolate the effect of a design parameter on the response by varying that particular parameter while holding the remaining ones constant. Two-dimensional slices of the responses are plotted to allow the user to visualize the impact of each parameter separately in real time. Including the uncertainty of the prediction gives the user more information to work with. For example, the predictive distribution can be used to select the next sample point in light of the current sample to pursue some goal, such as decreasing the output value or decreasing overall predictive uncertainty. Sacks et al. use an expected improvement criterion based on predictive interpolation uncertainty to drive sampling toward a global optimum[11]. Utilization of this visualization technique enables the uncertainty due to each parameter to be viewed separately, which

could lead to the discovery of the parameters responsible for the majority of the uncertainty. Future testing plans can be made more efficient by specifically targeting that parameter. Decision makers will then be more confident that a future test will decrease the level of uncertainty. A similar visualization can be done with the hyperparameters of the Gaussian process model to help assist the user in evaluating their impact as well. It should be made clear that the uncertainty shown by the Gaussian process model is not the true uncertainty of the model. It only shows the uncertainty relative to other areas in the design space and the uncertainty trends. However, this can still give the user valuable insight into the physics of the problem.

As an initial step in this research, the proposed method is tested on NACA 4-series airfoils as a proof of concept. These airfoils were chosen due to the information available regarding their aerodynamic performance from NACA wind tunnel experiments[12]. Some is utilized as a data set during the implementation of the method while the rest is used for validation. Once the method has been validated for this example, it will be applied to more representative real world problems such as open rotor in subsequent papers.

2 Technical Approach

Two key assumptions are made about the kind of problems for which this method could be used:

1. There is a limited amount of experimental data from prior feasibility studies.
2. The data is smooth, meaning the responses from two inputs located a short distance from each other are similar.

The diagram shown in Fig. 1 pictorially shows the process described in the following sections.

2.1 High Fidelity Correction

Once the data sets have been obtained or generated, a high fidelity correction surrogate is used

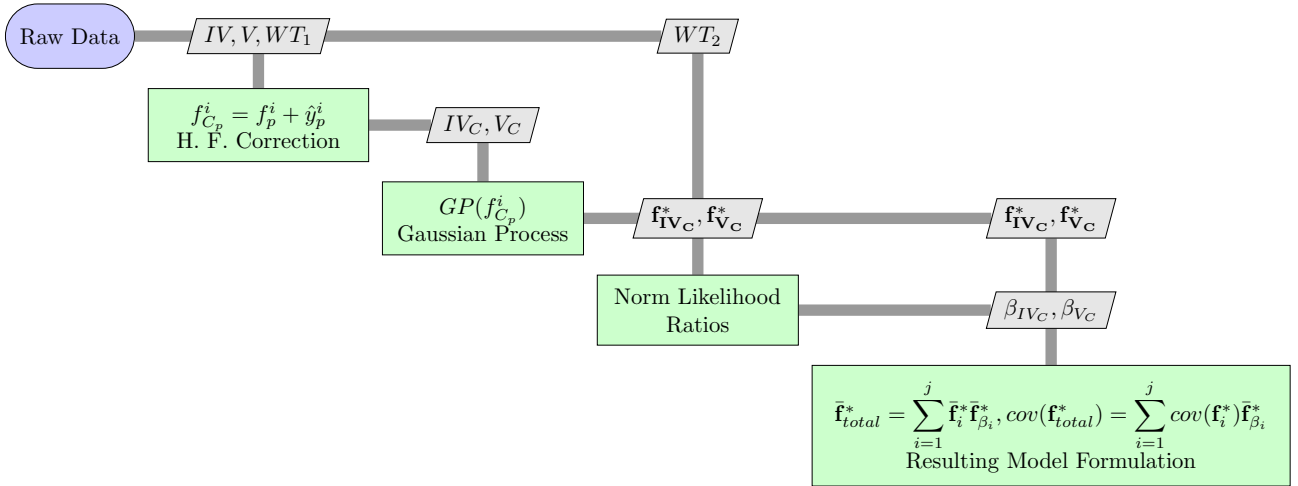


Fig. 1 XDSM representation of the technical approach[13]. Information in the green boxes represents general analysis steps described in Section 2, the gray boxes represent the data from the proof-of-concept described in section 3, and the dark gray lines represent the flow of data.

to remove the bias due to the assumptions in the lower fidelity data sets. This is an important step to ensure the ensemble method does not unfairly weight the higher fidelity data set. A subset of high fidelity data, sometimes referred to as the “truth model,” is used to create the correction surrogate for each data set. The correction surrogate is created by fitting a model to the difference between the high fidelity subset and the lower fidelity data at each high fidelity observation for each data set. However, there are typically a limited amount of data points in the high fidelity subset. It is challenging to fit an accurate surrogate to such a sparse data set because traditional multifidelity methods do not work well when the data set is small[14]. The authors found that a kriging interpolation model is able to fit the data best. The mean prediction from the kriging model becomes the correction surrogate.

Kriging models express an observer’s uncertainty about a response that has not yet been observed, based on a sample. The uncertainty due to lack of data has been termed “interpolation uncertainty” by Apley, Liu, and Chen [15] and “code uncertainty” by Kennedy and O’Hagan [16]. Kriging is given a Bayesian interpretation, or a type of surrogate model that is fit to an observed sample and yields a predictive probability distribution on the response at new input points.

In recent years, kriging has been studied extensively as a surrogate model for engineering design [3, 5, 17, 18].

The following brief description of kriging is based on the detailed explanations in Forrester et al. and Jones[5, 19]. Kriging predicts the value of a random field at a new input point from responses at nearby design points[20]. It begins with a set of sample data and their observed responses.

$$\underline{X} = \{\underline{x}_1, \underline{x}_2, \dots, \underline{x}_n\}^T \quad (1)$$

$$\underline{y} = \{y(\underline{x}_1), y(\underline{x}_2), \dots, y(\underline{x}_n)\}^T \quad (2)$$

The responses are assumed to be random vectors with a mean of $\mathbf{1}\mu$, where $\mathbf{1}$ is an $n \times 1$ column vector of ones. Subsequently, the kriging basis function is used to correlate the random variables:

$$\mathbf{R} = \text{Corr}[y(\underline{x}_p), y(\underline{x}_q)] = \exp\left(-\sum_{l=1}^D \lambda^l |\underline{x}_p^l - \underline{x}_q^l|^2\right) \quad (3)$$

where superscript l is used to denote the different design variables whereas subscripts p and q represent the observations. If the function is assumed to be continuous, the correlation function makes intuitive sense. The values at $y(\underline{x}_p)$ and

$y(\underline{x}_q)$ will tend to be close if $\|\underline{x}_p - \underline{x}_q\|$ is small. If $\underline{x}_p = \underline{x}_q$ then the correlation will be 1, and if $\|\underline{x}_p - \underline{x}_q\| \rightarrow \infty$, the correlation tends to zero. The λ^l hyperparameter represents the speed with which the correlation decays as one moves in the l^{th} variable direction. Large values of λ^l mean the function changes rapidly in the l^{th} variable direction. The correlations are then used to form a covariance matrix.

$$Cov(\mathbf{y}) = \sigma^2 \mathbf{R}. \quad (4)$$

The distribution of \mathbf{y} describes how the function is expected to change as each variable is changed. It depends on μ, σ^2 , and λ^l . Approximate parameters ($\hat{\mu}, \hat{\sigma}^2$, and $\hat{\lambda}^l$) are chosen such that they maximize the likelihood of the observed data. Essentially, these parameters are chosen such that the model represents the observed data as much as possible. Refer to Forrester et al. or Jones for the details of maximum likelihood estimation[5, 19].

To make predictions at some new point \underline{x}' , a value of y' is initially guessed. This new point (\underline{x}', y') is added to the system as the $(n + 1)$ observation and a new likelihood function, referred to as the augmented likelihood function, is computed based on the parameters found from the maximum likelihood estimation. The augmented likelihood function is only a function of y' , since the parameters $\hat{\mu}, \hat{\sigma}^2$, and $\hat{\lambda}^l$ are fixed. Therefore, the best predictor of y' is a value that maximizes the augmented likelihood function. Hence this value of y' becomes the kriging predictor. Let \mathbf{r} be the vector of correlations between $y(\underline{x}')$ and $y(\underline{x}_p)$, for $p = 1, \dots, n$.

$$\mathbf{r} = \begin{pmatrix} Corr[y(\underline{x}'), y(\underline{x}_1)] \\ \vdots \\ Corr[y(\underline{x}'), y(\underline{x}_n)] \end{pmatrix} \quad (5)$$

The correlation matrix for the augmented data set is:

$$\hat{\mathbf{R}} = \begin{pmatrix} \mathbf{R} & \mathbf{r} \\ \mathbf{r}' & 1 \end{pmatrix} \quad (6)$$

The augmented correlation matrix is then used to create the augmented likelihood function. To find the value of y' that maximizes the augmented likelihood function, the derivative of the

augmented likelihood function is taken and set equal to zero. Solving this function for y' results in the following formula for the kriging predictor.

$$\hat{y}(\underline{x}') = \hat{\mu} + \mathbf{r}' \mathbf{R}^{-1} (\mathbf{y} - \mathbf{1} \hat{\mu}) \quad (7)$$

The difference between the “truth model” observations and the lower fidelity predictions becomes the training data for the kriging model. The kriging predictor represents the correction surrogate which is then used to predict the difference between the “truth model” and the lower fidelity data set at every point in the lower fidelity data set. The predicted difference is then added to the lower fidelity data sets to form the corrected data sets shown in the equation below,

$$f_{C_p}^i = f_p^i + \hat{y}_p^i \quad (8)$$

where subscript C is used to represent the corrected data set.

2.2 Gaussian Process Regression

The next step is to fit the corrected data sets with a Gaussian process. A Gaussian process is a class of stochastic processes that, given a set of data, uses the multivariate Gaussian distribution to make predictions at unobserved locations in the input space. It is a statistically rigorous approach for constructing surrogate models of deterministic computer codes[21]. A Gaussian process is commonly derived from a Bayesian perspective, similar to kriging[22, 23]. Gaussian processes are also commonly referred to as kriging (depending on the kernel) or Design and Analysis of Computer Experiments (DACE)[24, 25]. The DACE approach was popularized by Sacks et al. and Cressie[11, 20]. The covariance of a Gaussian process, which is used as a representation of uncertainty, is mathematically defined based on a covariance function, also called a kernel. Different distance based kernels can be chosen based on the user’s preference. The present research uses the squared exponential kernel and a zero mean function which makes it mathematically similar to standard kriging[5, 20]. Choosing an intuitive distance based kernel helps bring the Gaussian process out of the abstract mathe-

mathematical world and into the physical engineering world.

Only a brief explanation of Gaussian processes is given in this report because of the similarities to kriging. The reason for using a Gaussian process instead of kriging again is because a Gaussian process is a regression formulation, and additional noise to represent model form uncertainty can be added easily. The reader is encouraged to read chapter 2 of *Gaussian Processes for Machine Learning* by Rasmussen and Williams for a more detailed explanation[21].

A Gaussian process is specified by its mean function $m(\underline{x})$ and covariance function $k(\underline{x}, \underline{x}')$ which are defined as

$$m(\underline{x}) = \mathbb{E}[f(\underline{x})] \quad (9)$$

$$k(\underline{x}, \underline{x}') = \mathbb{E}[(f(\underline{x}) - m(\underline{x}))(f(\underline{x}') - m(\underline{x}'))]. \quad (10)$$

The mean function is typically set to zero in practice. This also makes the derivation easier to follow. An additional noise variable is added into the regression model such that $y = f(\underline{x}) + \epsilon$. A decision maker can specify the amount of noise added to the simulation to represent the model form uncertainty. Assuming Gaussian noise ϵ with variance σ_n^2 , the prior becomes

$$\text{cov}(\mathbf{y}) = K(\underline{X}, \underline{X}) + \sigma_n^2 \mathbf{I}. \quad (11)$$

where \mathbf{I} is the identity matrix and $K(\underline{X}, \underline{X})$ is the $n \times n$ covariance matrix evaluated by the squared exponential covariance function, shown below.

$$\begin{aligned} \text{cov}(f(\underline{x}_p), f(\underline{x}_q)) &= k(\underline{x}_p, \underline{x}_q) = \\ &= \sigma_f^2 \exp\left(-\frac{1}{2\lambda^l} (\underline{x}_p^l - \underline{x}_q^l)^2\right) + \sigma_n^2 \delta_{pq} \end{aligned} \quad (12)$$

It should be noted that the covariance of the output is a function of the inputs. Also notice the similarities to Equation 3 from Section 2.1. The joint distribution of the observed values and the function values at the test locations is shown in the following equation.

$$\begin{bmatrix} \mathbf{y} \\ \mathbf{f}^* \end{bmatrix} \sim \mathcal{N}\left(0, \begin{bmatrix} K(\underline{X}, \underline{X}) + \sigma_n^2 \mathbf{I} & K(\underline{X}, \underline{X}^*) \\ K(\underline{X}^*, \underline{X}) & K(\underline{X}^*, \underline{X}^*) \end{bmatrix}\right) \quad (13)$$

The predictive equations for the Gaussian process regression are

$$\mathbf{f}^* | \underline{X}, \mathbf{y}, \underline{X}^* \sim \mathcal{N}(\bar{\mathbf{f}}^*, \text{cov}(\mathbf{f}^*)) \quad (14)$$

where

$$\bar{\mathbf{f}}^* = K(\underline{X}^*, \underline{X}) [K(\underline{X}, \underline{X}) + \sigma_n^2 \mathbf{I}]^{-1} \mathbf{y} \quad (15)$$

$$\begin{aligned} \text{cov}(\mathbf{f}^*) &= K(\underline{X}^*, \underline{X}^*) - K(\underline{X}^*, \underline{X}) \\ &\quad [K(\underline{X}, \underline{X}) + \sigma_n^2 \mathbf{I}]^{-1} K(\underline{X}, \underline{X}^*) \end{aligned} \quad (16)$$

The MATLAB code that accompanies the text by Rasmussen and Williams is used to generate the Gaussian process surrogate. The hyperparameters $(\lambda^1, \lambda^2, \dots, \lambda^D)$ are referred to as the characteristic length scale for each dimension. They show the degree of nonlinearity in the dimension they are associated with. Therefore, they can be used as a sensitivity study.

2.3 Model Combination

The models are now combined using a likelihood ratio test similar to Bayesian model averaging[26, 27]. A second set of high fidelity data, or ‘‘truth model,’’ is used to determine a variable weighting factor β for the lower fidelity data sets. It is important to note that this second high fidelity data set is not the same data set used to create the correction surrogates in Section 2.1. First, a likelihood is computed for each Gaussian process at every high fidelity observation. The weighting at each observation is determined by calculating the normalized likelihood for each data set as shown by the equation below.

$$\beta_i = \frac{\text{lik}_i}{\sum_{i=1}^j \text{lik}_i} \quad (17)$$

Another Gaussian process regression is then fit to weighting factors for each data set. The mean prediction from the regression represents

the variable weighting factor model. To get the combined mean and covariance, the individual means and covariances are multiplied by their respective weighting factors and then added together.

$$\bar{\mathbf{f}}_{total}^* = \sum_{i=1}^j \bar{\mathbf{f}}_i^* \bar{\mathbf{f}}_{\beta_i}^* \quad (18)$$

$$cov(\mathbf{f}_{total}^*) = \sum_{i=1}^j cov(\mathbf{f}_i^*) \bar{\mathbf{f}}_{\beta_i}^* \quad (19)$$

3 Proof of Concept

The proposed method is implemented in MATLAB on NACA 4-series airfoils. The method attempts to predict the lift coefficient, C_l , as a function of the three NACA 4-series geometry parameters and the angle of attack, α . All geometry parameters are normalized by the chord. A total of 48 wind tunnel observations from *Theory of Wing Sections* by Abbott and Doenhoff[12] are used as the “truth models” to generate the high fidelity design space. Additional lower fidelity data sets are generated using XFOIL, which is a potential flow solver that can optionally include an interactive integral boundary layer formulation and stability model[28]. The lower fidelity data set is generated using incompressible inviscid simulations and the higher fidelity data is generated using incompressible viscous simulations.

A MATLAB script was set up to perform a sweep of all the input parameters in XFOIL while holding the Reynolds number constant at 6 million for the viscous cases. The viscous data set is smaller to simulate a more realistic problem where an engineer could likely generate lots of low fidelity data and a smaller amount of higher fidelity data along with a limited amount of experimental data. See Tables 1 and 2 for a list of the parameter ranges used for each data set. This results in 675 data points for the inviscid set and 105 points for the viscous set.

Observations for the NACA 0006, 0012, 1408, 2418, and 4424 airfoils make up the first wind tunnel set, WT_1 , and are used to create the correction surrogates. Fig. 2 compares the predictive capability of the corrected and uncor-

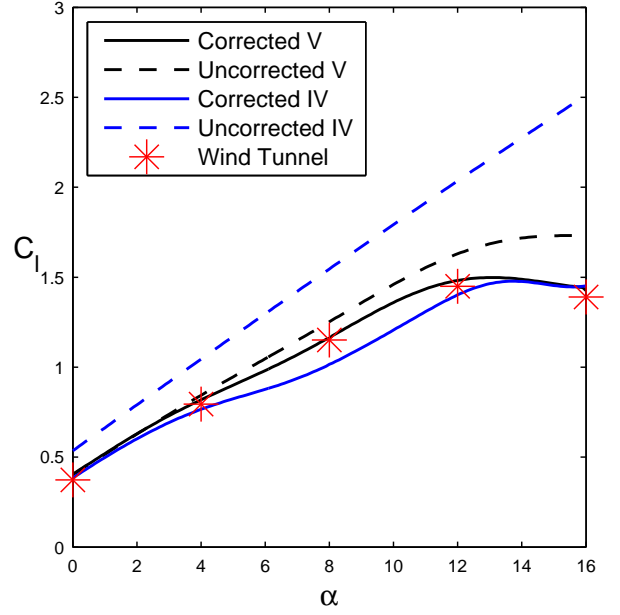


Fig. 2 Lift curve predictions of a NACA 4418 airfoil with and without the correction surrogates for the viscous (V) and inviscid (IV) data sets. The wind tunnel results are shown in red as a reference.

Table 1 Input parameter ranges for inviscid XFOIL simulations

	Lower Bound	Upper Bound	Step
Max Camber	0	4	1
Max Camber Location	0	4	1
Thickness Ratio	6%	24%	2%
Angle of Attack	0	16	4

Table 2 Input parameter ranges for Viscous XFOIL simulations

	Lower Bound	Upper Bound	Step
Max Camber	0	4	2
Max Camber Location	0	4	2
Thickness Ratio	6%	24%	6%
Angle of Attack	0	16	8

rected data sets for a NACA 4418. The wind tunnel observations for the NACA 4418 are represented by the red stars. Notice how each correction surrogate significantly improves the prediction. The equations for the corrected data sets are shown below, where subscript V and IV refer to the viscous and inviscid data sets respectively.

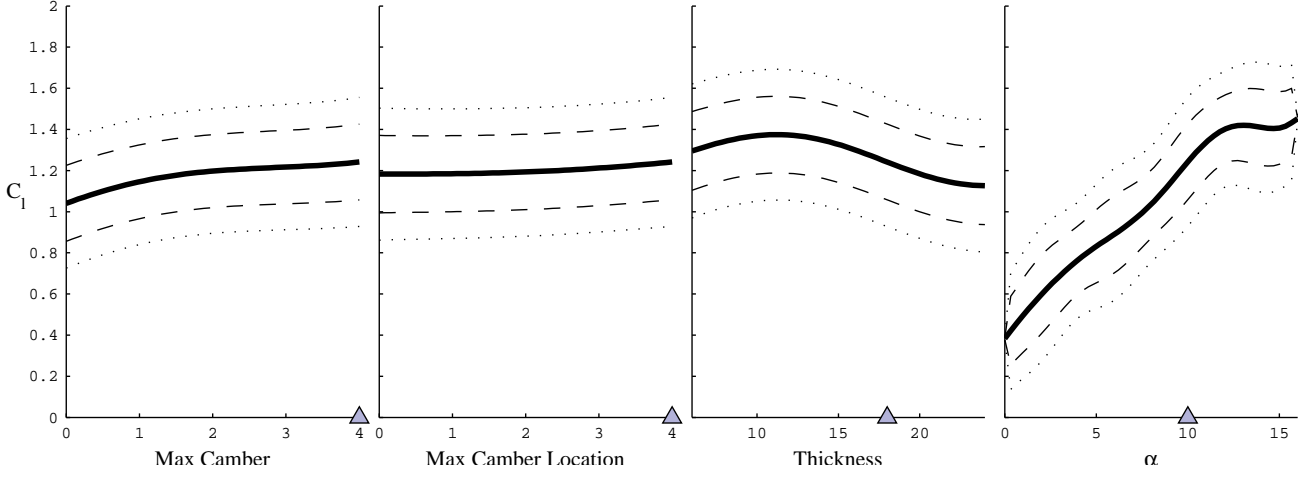


Fig. 3 NACA 4418 airfoil using only the corrected inviscid Gaussian process surrogate, f_{IVc} .

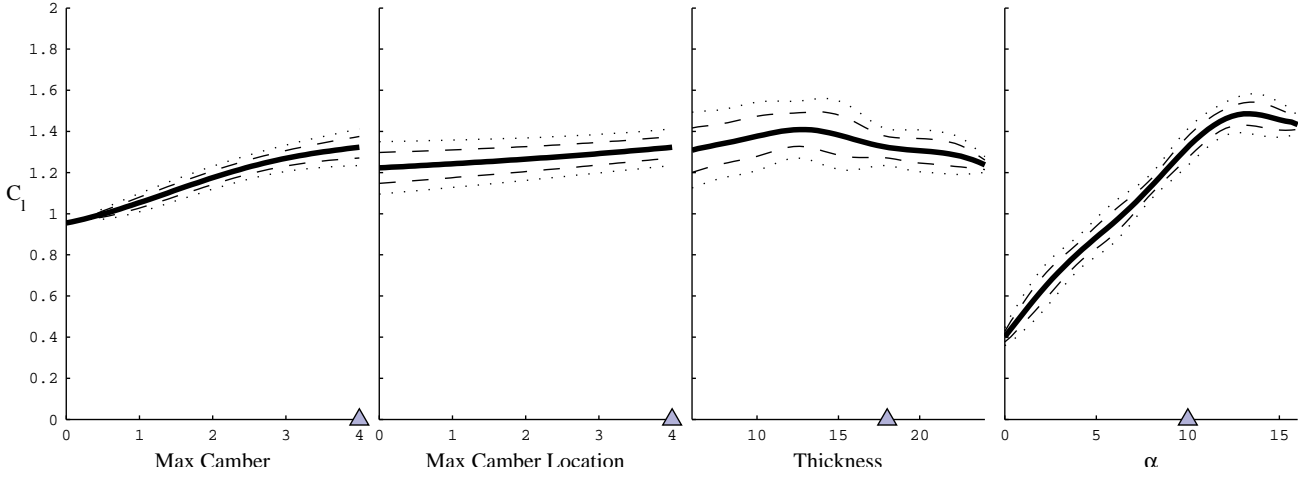


Fig. 4 NACA 4418 airfoil using the combined Gaussian process surrogate, f_{total}^* .

$$V_{C_p}^i = V_p^i + \hat{y}_{V_p}^i \quad (20)$$

$$IV_{C_p}^i = IV_p^i + \hat{y}_{IV_p}^i \quad (21)$$

The corrected data sets are then fit with a Gaussian process and combined using the ensemble method described earlier. Applying equations 17,18, and 19 to the corrected XFOIL data sets results to the following,

$$\beta_{IV}^k = \frac{lik_{IV}^k}{lik_{IV}^k + lik_V^k} \quad (22)$$

$$\beta_V^k = \frac{lik_V^k}{lik_{IV}^k + lik_V^k} \quad (23)$$

$$\bar{\mathbf{f}}_{total}^* = \bar{\mathbf{f}}_{IV}^* \bar{\mathbf{f}}_{\beta_{IV}}^* + \bar{\mathbf{f}}_V^* \bar{\mathbf{f}}_{\beta_V}^* \quad (24)$$

$$cov(\mathbf{f}_{total}^*) = cov(\mathbf{f}_{IV}^*) \bar{\mathbf{f}}_{\beta_{IV}}^* + cov(\mathbf{f}_V^*) \bar{\mathbf{f}}_{\beta_V}^* \quad (25)$$

Wind tunnel observations for the NACA 0010, 2408, 2415, and 4421 are used as the high fidelity data for the ensemble method. The resulting surrogate can now be utilized for parametric design space exploration.

4 Results and Discussion

The following discussion is based on the prediction of the lift curve for a NACA 4418 airfoil. However, it should be noted that one of the key advantages of creating a surrogate to represent the entire high fidelity design space is that it allows the user to quickly generate multiple predictions which allows for rapid parametric design space exploration.

A dynamic sensitivity derivative visualization environment was set up in MATLAB to help visualize the sensitivity of the response to the individual parameters. Fig. 3 shows this visualization for the NACA 4418 airfoil using only the corrected inviscid Gaussian process surrogate, f_{IVC} .

The various inputs (maximum camber, maximum camber location, etc.) are listed along the independent axes, and the response, C_l , is on the dependent axis. The reader can think of these plots as partial derivatives because they show the impact of one specific parameter on the response while holding the others fixed. The solid lines represent the mean prediction, while the dashed and dotted lines represent one and two standard deviations respectively. The triangles at the bottom of each plot indicate the current setting for each parameter. For instance 4, 4, and 18 for the geometry parameters, and 10° for the angle of attack. The last plot in Fig. 3 is the predicted lift curve for the NACA 4418. Notice how the uncertainty in the plots is close to uniform. This indicates that the accuracy of the prediction is dominated by the artificial noise that was added to account for the model form uncertainty described in Section 2.2.

Fig. 4 shows the sensitivity derivatives for the NACA 4418 airfoil using the combined Gaussian process surrogate. Notice the uncertainty decreases at locations near viscous observations i.e. 0° , 8° , and 16° on the lift curve. Refer to Tables 1 and 2 for more specifics on the locations of the data points.

Fig. 5 again shows the predicted lift curve for the NACA 4418 for the final surrogate, but it also includes the predicted lift curves for the corrected viscous and inviscid data sets as well as the true wind tunnel observations as a comparison. Notice how the corrected viscous prediction gives a more accurate prediction. The ensemble method realizes this and automatically weights the viscous data set more in this area of the design space. On the other hand, the opposite is true for the NACA 4412. The predicted lift curves of a NACA 4412 shown in Figure 6 indicate that the corrected inviscid data set is more accurate. It may seem counter intuitive to the reader for the

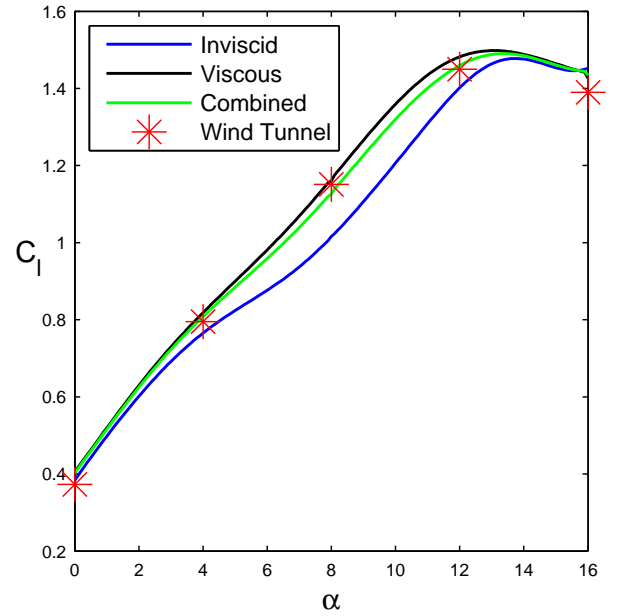


Fig. 5 Lift curve predictions of a NACA 4418 airfoil for the corrected inviscid (f_{IVC}) and viscous (f_{VC}) data sets as well as the combined surrogate. The wind tunnel results are shown in red as a reference.

inviscid data set to be more accurate in certain areas of the design space. This is due to the fact that the viscous data set is much smaller; therefore, there is a lack of viscous data in some areas. It may also be a result of a better correction surrogate in some areas of the design space. The advantage of the ensemble method used is that it accounts for this switch in fidelity level throughout the design space.

An attempt was also made to extrapolate beyond the bounds of the data sets. Fig. 7 again shows the predicted lift curve for the NACA 4418 like Fig. 5, but this time the models attempt to predict the lift curve up to 20° angle of attack. Notice how the predictions continue upwards away from the true value after 16° angle of attack. Therefore, this method should not be used to extrapolate beyond the boundaries of the data.

The research presented in this paper has shown how a Gaussian process can be used as a representation of uncertainty. The reader should be aware that this is not a representation of the

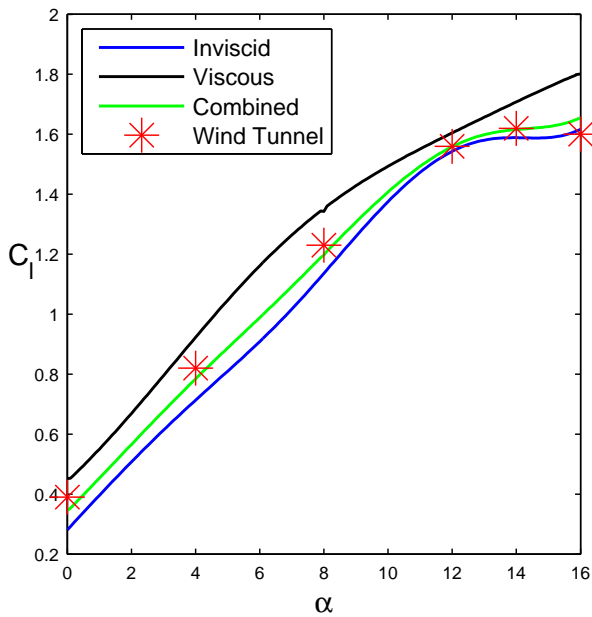


Fig. 6 Lift curve predictions of a NACA 4412 airfoil for the corrected inviscid (f_{IV_C}) and viscous (f_{V_C}) data sets as well as the combined surrogate. The wind tunnel results are shown in red as a reference.

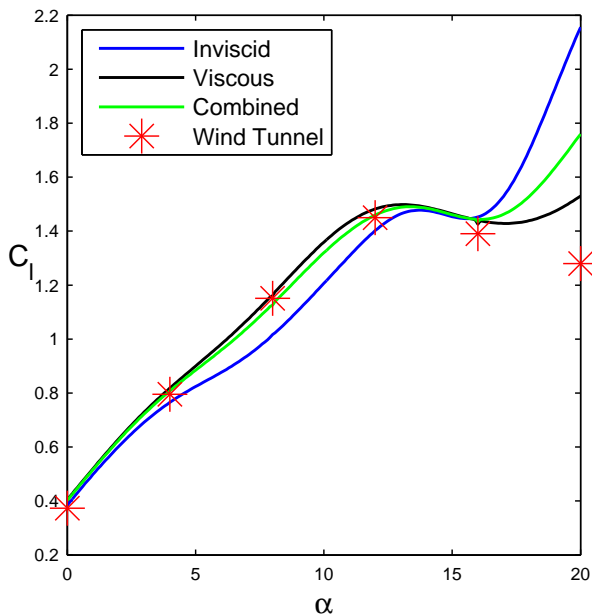


Fig. 7 Extrapolated lift curve predictions of a NACA 4418 airfoil for the corrected inviscid (f_{IV_C}) and viscous (f_{V_C}) data sets as well as the combined surrogate (f_{total}^*). The wind tunnel results are shown in red as a reference.

true uncertainty. However, it does indicate the relative uncertainty. Meaning that areas in the design space where the uncertainty is higher relative to other areas, would also have a higher actual uncertainty.

The results indicate that using an ensemble method to combine Gaussian process surrogates of multiple data sets gives an improved high fidelity design space representation.

References

- [1] Collier, F., Thomas, R., Burley, C., Nickol, C., Lee, C.-m., and Tong, M., “Environmentally Responsible Aviation - Real Solutions For Environmental Challenges Facing Aviation,” *27th International Congress of the Aeronautical Sciences*, Nice, 2010.
- [2] Hager, R. D. and Vrabel, D., “Advance Turbo-prop Project,” *NASA SP-495*, 1988.
- [3] Keane, A. J., “Cokriging for Robust Design Optimization,” *AIAA Journal*, Vol. 50, No. 11, Nov. 2012, pp. 2351–2364.
- [4] March, A. and Willcox, K., “Multifidelity Approaches for Parallel Multidisciplinary Optimization,” *12th AIAA Aviation Technology, Integration, and Operations (ATIO) Conference*, No. September, Indianapolis, 2012, pp. 1–23.
- [5] Forrester, A. I. J., Sóbester, A., and Keane, A. J., *Engineering Design via Surrogate Modelling: A Practical Guide*, John-Wiley and Sons, 2008.
- [6] Simpson, T. W., Lin, D. K. J., and Chen, W., “Sampling Strategies for Computer Experiments: Design and Analysis,” *International Journal of Reliability and Applications*, Vol. 2, No. 3, 2001, pp. 209–240.
- [7] Zang, T. A., Hemsch, M. J., Hilburger, M. W., Kenny, S. P., Luckring, J. M., Maghami, P., Padula, S. L., and Stroud, W. J., “Needs and Opportunities for Uncertainty-Based Multidisciplinary Design Methods for Aerospace Vehicles,” Tech. Rep. July, NASA, 2002.
- [8] Yao, W., Chen, X., Luo, W., van Tooren, M., and Guo, J., “Review of uncertainty-based multidisciplinary design optimization methods for aerospace vehicles,” *Progress in Aerospace Sciences*, Vol. 47, No. 6, Aug. 2011, pp. 450–479.
- [9] Oberkampf, W. L. and Roy, C. J., *Verification*

- and Validation in Scientific Computing*, Cambridge University Press, New York, 2010.
- [10] Kennedy, M. C. and O'Hagan, A., "Predicting the output from a complex computer code when fast approximations are available," *Biometrika*, Vol. 87, 2000, pp. 1–13.
- [11] Sacks, J., Welch, W. J., Mitchell, T. J., and Wynn, H. P., "Design and Analysis of Computer Experiments," *Statistical Science*, Vol. 4, No. 4, 1989, pp. 409–435.
- [12] Abbott, I. H. and Von Doenhoff, A. E., *Theory Of Wing Sections*, Dover Publications, New York, 1959.
- [13] Lambe, A. B. and Martins, J. R. R. a., "Extensions to the design structure matrix for the description of multidisciplinary design, analysis, and optimization processes," *Structural and Multidisciplinary Optimization*, Vol. 46, No. 2, Jan. 2012, pp. 273–284.
- [14] Viana, F. A. C., Simpson, T. W., Balabanov, V., and Toropov, V., "Metamodeling in Multidisciplinary Design Optimization: How Far Have We Really Come?" *AIAA Journal*, Vol. 52, No. 4, April 2014, pp. 670–690.
- [15] Apley, D. W., Liu, J., and Chen, W., "Understanding the Effects of Model Uncertainty in Robust Design With Computer Experiments," *Journal of Mechanical Design*, Vol. 128, No. 4, 2006, pp. 945.
- [16] Kennedy, M. C. and O'Hagan, A., "Bayesian Calibration of Computer Models," *Journal of the Royal Statistical Society: Series B (Statistical Methodology)*, Vol. 63, No. 3, 2001, pp. 425–464.
- [17] Martin, J. D. and Simpson, T. W., "Use of Kriging Models to Approximate Deterministic Computer Models," *AIAA Journal*, Vol. 43, No. 4, April 2005, pp. 853–863.
- [18] Laurenceau, J. and Sagaut, P., "Building Efficient Response Surfaces of Aerodynamic Functions with Kriging and Cokriging," *AIAA Journal*, Vol. 46, No. 2, Feb. 2008, pp. 498–507.
- [19] Jones, D. R., "A Taxonomy of Global Optimization Methods Based on Response Surfaces," *Journal of global optimization*, Vol. 21, 2001, pp. 345–383.
- [20] Cressie, N., "The Origins of Kriging," *Mathematical Geology*, Vol. 22, No. 3, 1990, pp. 239–252.
- [21] Rasmussen, C. E. and Williams, C. K. I., *Gaussian Processes for Machine Learning*, MIT Press, 2006.
- [22] Currin, C., Mitchell, T., Morris, M., and Ylvisaker, D., "Bayesian Prediction of Deterministic Functions, With Applications to the Design and Analysis of Computer Experiments," *Journal of the American Statistical Association*, Vol. 86, No. 416, 1991, pp. 953–963.
- [23] Neal, R. M., "Regression and Classification Using Gaussian Process Priors," *Bayesian Statistics 6*, edited by J. M. Bernardo, J. O. Berger, A. P. Dawid, and A. F. M. Smith, Oxford University Press, 1998, pp. 475–501.
- [24] Keane, A. J. and Nair, P. B., *Computational Approaches for Aerospace Design: The Pursuit of Excellence*, John-Wiley and Sons, West Sussex, 2005.
- [25] Cressie, N. A. C., *Statistics for Spatial Data*, John-Wiley and Sons, New York, 1993.
- [26] Wasserman, L., "Bayesian Model Selection and Model Averaging," *Journal of mathematical psychology*, Vol. 44, No. 1, March 2000, pp. 92–107.
- [27] Hoeting, J. A., Madigan, D., Raftery, A. E., and Volinsky, C. T., "Bayesian Model Averaging : A Tutorial," *Statistical Science*, Vol. 14, No. 4, 1999, pp. 382–417.
- [28] Drela, M. and Youngren, H., "Xfoil 6.9 User Primer," 2001.

5 Contact Author Email Address

Henry D. Schwartz
mailto:hschwartz3@gatech.edu

Copyright Statement

The authors confirm that they, and/or their company or organization, hold copyright on all of the original material included in this paper. The authors also confirm that they have obtained permission, from the copyright holder of any third party material included in this paper, to publish it as part of their paper. The authors confirm that they give permission, or have obtained permission from the copyright holder of this paper, for the publication and distribution of this paper as part of the ICAS 2014 proceedings or as individual off-prints from the proceedings.